Remote Sounding of Cloud Parameters from a Combination of Infrared and Microwave Channels

HWA-YOUNG YEH[1] AND KUO-NAN LIOU

Department of Meteorology, University of Utah, Salt Lake City 84112

(Manuscript received 1 June 1982, in final form 1 November 1982)

ABSTRACT

This study explores the utilization of both infrared and microwave sounding channels for the inference of the high and low cloud parameters. The necessary parameterized equations for infrared and microwave radiative transfer have been derived for applications to remote sensing from satellites. Retrieval programs have been developed for the determination of the high cloud top height, high cloud thickness, low cloud top height, surface emissivities, and cloud liquid water content successively from a set of HIRS and SCAMS channels. Analyses involving random errors in the assumed temperature and water vapor profiles and measurement errors in the theoretically computed radiances and brightness temperatures have been carried out to investigate the sensitivity of these errors on the retrieval program. Results of error analyses reveal that the cloud retrieval technique developed in this paper appears to be theoretically rigorous and practically feasible. The retrieval technique is then applied to Nimbus 6 HIRS and SCAMS data for a number of carefully selected cases associated with summertime convective cloud systems. Results of the satellite retrieved cloud parameters based on a combination of infrared and microwave channels appear to be in qualitative agreement with the available synoptic, surface and radar observations.

1. Introduction

Remote sounding of cloud parameters from orbiting meteorological satellites has gained increasing attention in recent years because of the urgent need for new cloud climatology including information on the cloud cover and vertical structure and compositions. Knowledge of the horizontal and vertical distributions and the optical properties of globally distributed clouds is of fundamental importance to the understanding of the radiation and heat balance, weather and climate of the earth and the atmosphere. Although broadband radiometers such as those on the NOAA series of satellites have been used extensively to derive cloud cover, study of the quantitative estimate of the vertical cloud composition and structure by means of passive remote satellite sounding has been extremely limited because of the complexity of the cloud interaction with the radiation field of the atmosphere.

In recent years, several investigations have specifically aimed at the exploration of sounding capabilities utilizing infrared frequencies. Houghton and Hunt (1971) explored the feasibility of remote sensing of ice clouds by utilizing two wavelengths in the far infrared. Smith and Woolf (1976) presented a statistical covariance method for inferring the cloud altitude and amount using the HIRS data. Liou (1977) proposed a theoretical retrieval technique to infer the fraction of cirrus cloud cover and cloud thickness by means of four radiance measurements in the 10 μm window region. McCleese and Wilson (1976) and Chahine *et al.* (1977) demonstrated that cloud heights and amounts can be recovered using infrared frequencies in the CO_2 absorption bands. Feddes and Liou (1978) derived the ice and water content of high and middle clouds from parameterization of Nimbus 6 HIRS data using a combination of water vapor and carbon dioxide channels. More recently, Wielicki and Coakley (1981) presented a feasibility study for cloud top height and cloud amount retrieval using infrared sounder data. However, owing to the large opacity in the infrared region, it would be difficult to derive the liquid water content and thickness information of low clouds or clouds composed of water droplets.

Applications of microwave radiometry to remote sensing of atmospheric liquid water and water vapor have been studied using data gathered by Nimbus 5 and 6 satellites. The prime advantage of microwave over infrared frequencies is that the longer wavelength microwaves can penetrate through precipitating and nonprecipitating low clouds. Grody (1976) and Staelin *et al.* (1976) used linear empirical equations based on regression analyses to infer the water content from Nimbus 5 NEMS channels over ocean. Liou and Duff (1979) developed an empirical-theo-

[1] Present affiliation: Cooperative Institute for Research in the Atmosphere (CIRA), Colorado State University, Fort Collins 80523.

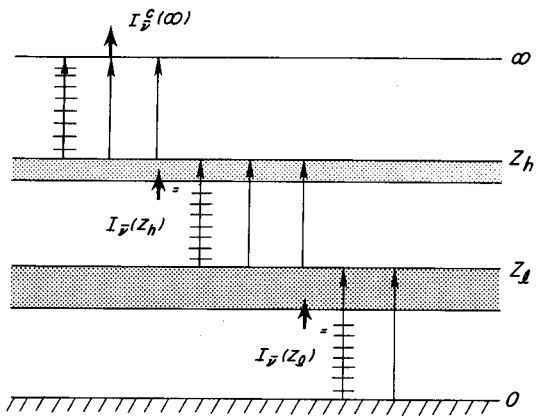

FIG. 1. Configuration of the upwelling infrared radiance at the top of the atmosphere in terms of the cloud and atmospheric radiance contributions.

retical method to determine liquid water content over land from the Nimbus 6 SCAMS data. More recently, Grody *et al.* (1980) further developed high-order equations to infer water content over the tropical Pacific from Nimbus 6 SCAMS channels.

Since low clouds are practically opaque in the infrared sounding frequencies and since high clouds are transparent in the microwave regions, it would appear that a proper combination of infrared and microwave measurements could result in useful and significant data for determining the vertical cloud structure and composition in all weather conditions. In this paper, we wish to demonstrate the feasibility of utilizing a combination of infrared and microwave sounding data for the inference of cloud parameters, based on a theoretical parameterization approach. In Section 2, we develop and derive the necessary parameterization equations for infrared and microwave radiation transfer in conjunction with the inference of cloud parameters from satellites. In Section 3, we present the successive retrieval programs for the determination of the high cloud top height, high cloud thickness, low cloud top height and liquid water content utilizing a number of appropriate HIRS and SCAMS channels. Results of the theoretical sensitivity analysis are described in Section 4. In Section 5, we apply the present sounding technique to the Nimbus 6 HIRS and SCAMS data invovling a summertime convective cloud system. Finally, the conclusion is presented in Section 6.

2. Parameterization of infrared and microwave radiation transfer in cloudy atmospheres

a. Infrared

We consider an overcast atmosphere containing two cloud layers. In reference to Fig. 1, we wish to derive the upwelling radiance at the top of the atmosphere in terms of the cloud and atmospheric radiative properties. This radiance is caused by 1) the transmission of the upwelling radiance from the high cloud, 2) the emission from the cloud top, and 3) the emission and absorption contribution of the gases above the cloud top. In terms of the mathematical expression, we write

$$I_{\bar{\nu}}^{c}(\infty) \approx \{I_{\bar{\nu}}(z_h)T_{\bar{\nu}}^{hc} + B_{\bar{\nu}}[T(z_h)](1 - T_{\bar{\nu}}^{hc})\}T_{\bar{\nu}}(\infty, z_h) + \int_{z_h}^{\infty} B_{\bar{\nu}}[T(z)]K_{\bar{\nu}}(\infty, z)dz, \quad (1)$$

where $T_{\bar{\nu}}^{hc}$ represents the high cloud transmissivity which is a function of the cloud thickness and optical property, $B_{\bar{\nu}}$ is the spectral Planck function at wavenumber $\bar{\nu}$, z_h the high cloud top, $T_{\bar{\nu}}$ the spectral transmittance for the relevant gas, $K_{\bar{\nu}} = dT_{\bar{\nu}}/dz$ the spectral weighting function, and the upwelling radiance from the high cloud may be expressed in terms of the radiative parameter for the low cloud as (see Fig. 1)

$$I_{\bar{\nu}}(z_h) \approx \{I_{\bar{\nu}}(z_l)T_{\bar{\nu}}^{lc} + B_{\bar{\nu}}[T(z_l)](1 - T_{\bar{\nu}}^{lc})\}T_{\bar{\nu}}(z_h, z_l) + \int_{z_l}^{z_h} B_{\bar{\nu}}[T(z)]K_{\bar{\nu}}(z_h, z)dz, \quad (2)$$

where $T_{\bar{\nu}}^{lc}$ denotes the low cloud transmissivity and z_l the low cloud top height. Finally, the upwelling radiance reaching the low cloud layer is (see Fig. 1)

$$I_{\bar{\nu}}(z_l) = B_{\bar{\nu}}(T_s)T_{\bar{\nu}}(z_l, 0) + \int_{0}^{z_l} B_{\bar{\nu}}[T(z)]K_{\bar{\nu}}(z_l, z)dz, \quad (3)$$

where T_s is the surface temperature. In writing the preceding equations, the surface infrared emissivity is assumed to be unity, the cloud reflectivity is considered to be negligible, and the cloud radiative properties are described by the cloud transmissivities which depend on the temperature structure and the amount of water in gaseous, liquid and/or ice forms.

Next we change the reference layer of clear column transmittances and weighting functions from high and low cloud layers to the top of the atmosphere in the forms

$$\left.\begin{aligned} T_{\bar{\nu}}(z_l, 0) &= T_{\bar{\nu}}(\infty, 0)/[T_{\bar{\nu}}(\infty, z_h)T_{\bar{\nu}}(z_h, z_l)] \\ K_{\bar{\nu}}(z_l, z) &= K_{\bar{\nu}}(\infty, z)/[T_{\bar{\nu}}(\infty, z_h)T_{\bar{\nu}}(z_h, z_l)], \\ &\qquad 0 < z < z_l \\ K_{\bar{\nu}}(z_h, z) &= K_{\bar{\nu}}(\infty, z)/T_{\bar{\nu}}(\infty, z_h), \\ &\qquad z_l < z < z_h \end{aligned}\right\}. \quad (4)$$

Strictly speaking, these relationships are based upon the monochromatic assumption on the transmittance calculations. However, we have carried out numerical computations using transmittances for CO_2 and H_2O channels and have found that these relationships are valid within about 1%.

On substituting Eqs. (2), (3) and (4) into Eq.

(1), and defining $T_{\bar{\nu}}(\infty, z) = T_{\bar{\nu}}(z)$ and $K_{\bar{\nu}}(\infty, z) = K_{\bar{\nu}}(z)$ for simplicity, we obtain a parameterized equation for the upwelling radiance emergent from a two-layer cloud model in the form

$$I^c_{\bar{\nu}}(\infty) = T^{hc}_{\bar{\nu}} T^{lc}_{\bar{\nu}} \Big[B_{\bar{\nu}}(0)T_{\bar{\nu}}(0) + \int_0^{z_l} B_\nu(z)K_{\bar{\nu}}(z)dz - B_{\bar{\nu}}(z_l)T_{\bar{\nu}}(z_l) \Big] + T^{hc}_{\bar{\nu}} \Big[\int_{z_l}^{z_h} B_{\bar{\nu}}(z)K_{\bar{\nu}}(z)dz + B_{\bar{\nu}}(z_l)T_{\bar{\nu}}(z_l) - B_{\bar{\nu}}(z_h)T_{\bar{\nu}}(z_h) \Big] + \Big[B_{\bar{\nu}}(z_h)T_{\bar{\nu}}(z_h) + \int_{z_h}^{\infty} B_{\bar{\nu}}(z)K_{\bar{\nu}}(z)dz \Big], \quad (5)$$

where the temperature contained in the Planck function is replaced by the corresponding height. In Eq. (5), the three terms on the right-hand side represent, respectively, the emission and absorption contributions from below the low cloud, from between the clouds and from above the high cloud.

In the absence of high cloud, $T^{hc}_{\bar{\nu}} = 1$ and $z_h = z_l$, and Eq. (5) reduces to

$$I^{lc}_{\bar{\nu}}(\infty) = T^{lc}_{\bar{\nu}} \Big[B_{\bar{\nu}}(0)T_{\bar{\nu}}(0) + \int_0^{z_l} B_{\bar{\nu}}(z)K_{\bar{\nu}}(z)dz \Big] + (1 - T^{lc}_{\bar{\nu}})B_{\bar{\nu}}(z_l)T_{\bar{\nu}}(z_l) + \int_{z_l}^{\infty} B_{\bar{\nu}}(z)K_{\bar{\nu}}(z)dz. \quad (6)$$

Likewise, if low cloud is absent, then Eq. (5) becomes

$$I^{hc}_{\bar{\nu}}(\infty) = T^{hc}_{\bar{\nu}} \Big[B_{\bar{\nu}}(0)T_{\bar{\nu}}(0) + \int_0^{z_h} B_{\bar{\nu}}(z)K_{\bar{\nu}}(z)dz \Big] + (1 - T^{hc}_{\bar{\nu}})B_{\bar{\nu}}(z_h)T_{\bar{\nu}}(z_h) + \int_{z_h}^{\infty} B_{\bar{\nu}}(z)K_{\bar{\nu}}(z)dz. \quad (7)$$

Under no cloud conditions, $T^{hc}_{\bar{\nu}} = T^{lc}_{\bar{\nu}} = 1$ and $z_h = z_l = 0$, and we find

$$I^{nc}_{\bar{\nu}}(\infty) = B_{\bar{\nu}}(0)T_{\bar{\nu}}(0) + \int_0^{\infty} B_{\bar{\nu}}(z)K_{\bar{\nu}}(z)dz. \quad (8)$$

This is the expression for clear column radiance. Eq. (5) is the fundamental parameterized transfer equation in the infrared region to be used for the inference of the cloud thicknesses and top heights.

b. Microwave

In the preceding subsection, we approximated the transfer of infrared radiation in an atmosphere containing high and low cloud layers based on the geometric consideration in which the cloud radiative properties are parameterized in terms of their bulk transmissivity. However, infrared radiation emitted from below the low cloud generally will not penetrate through the cloud because of its large opacity. The upwelling radiance that is observed above the low cloud is usually the emitted component from the cloud top portion. Thus, in order to estimate the low cloud properties, appropriate microwave frequencies are needed and we wish to derive a parameterized equation which may serve the purpose of the cloud parameter inference.

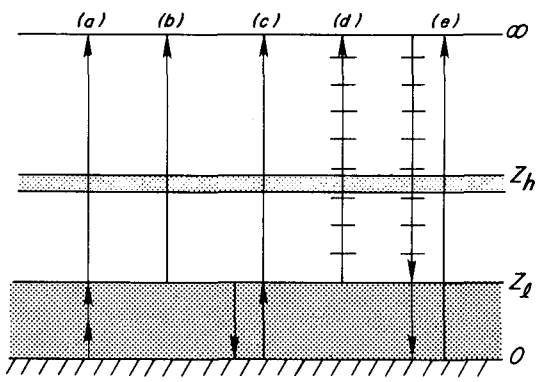

FIG. 2. Contributions of the upwelling brightness temperature in a cloudy atmosphere.

Since high clouds are transparent in the microwave region, it suffices to consider an atmosphere containing an overcast low cloud. Moreover, we assume that the cloud base is close to the surface so that the cloud top height is the thickness of the cloud. Under these restricted conditions, the upwelling brightness temperature in cloudy atmospheres at the satellite point may be decomposed into five sources as schematically illustrated in Fig. 2. These are (i) the direct contribution from the surface, (ii) the ground reflection of the cloud emission from below the cloud, (iii) emission from the cloud layer, (iv) the gaseous emission from the atmosphere above the cloud, and (v) ground reflection of gaseous emission above the cloud. Thus, the brightness temperature in cloudy atmospheres may be expressed in terms of a parameterized equation in the form

$$\tilde{T}_B(\nu) = \{[\epsilon_\nu T_s + \epsilon^c_\nu T_c(1 - \epsilon_\nu)]T^c_\nu + \epsilon^c_\nu T_c\} T_\nu(z_l) + \int_{z_l}^{\infty} T(z)K_\nu(z)dz + (T^c_\nu)^2(1 - \epsilon_\nu) \times \int_{z_l}^{\infty} [T_\nu(z_l)/T_\nu(z)]^2 T(z)K_\nu(z)dz, \quad (9)$$

where ϵ^c_ν denotes the cloud emissivity for a given average cloud temperature, ϵ_ν is the surface emissivity, T^c_ν the cloud transmissivity ($\approx 1 - \epsilon^c_\nu$), T_c the average cloud temperature which is assumed to be the same as the average ambient temperature, T_ν the gaseous transmittance, z_l the low cloud top height, and $K_\nu(z)$ the weighting function which is in reference to the top of the atmosphere. Eq. (9) is a parameterized equation relating the brightness temperature with the atmospheric and cloud parameters. Since a number

of assumptions are utilized in the formulation, the brightness temperature derived from this equation requires verifications which will be discussed in the last portion of this section.

For the cloud parameter inference, it is necessary at this point to further express the cloud emissivity and transmissivity in terms of certain mathematical functions in which the cloud thickness and/or cloud liquid water content are explicitly given. Using a microwave radiative transfer program developed at the University of Utah, analyses have been carried out to determine the relationships between the cloud emissivity and transmissivity and the cloud parameters. The microwave radiative transfer program utilizes the discrete-ordinates method for inhomogeneous atmospheres in which the cloud is considered to be non-isothermal and the gaseous absorption contribution within the cloud is also taken into consideration in the transfer calculation. The required input parameters for the microwave radiative transfer program are the extinction coefficient, single scattering albedo, and Legendre polynomial coefficients as calculated from a Mie scattering program. These optical parameters depend critically on the liquid water content which in turn is related to the drop size distribution. In addition, the cloud thickness, surface emissivity, and atmospheric temperature and moisture profiles are needed for the computation. For a given atmospheric temperature and humidity profile, the cloud thickness and rainfall rate are varied from 0.5 to 5 km and from 1 to 10 mm h^{-1}. On the basis of the raindrop size distribution given by Marshall and Palmer (1948), a unique relationship between the rainfall rate and cloud liquid water content (g m^{-3}) may be derived for a given cloud thickness.

On the basis of a number of numerical studies, the cloud emissivity and transmissivity can be expressed in terms of low-order polynomials containing liquid water content Δw and cloud thickness Δz. The number of terms in polynomials are determined by numerical trial and error in which a multiple regression program was employed to determine the accuracy of the simulated values using the parameterized equation. The final functions that we derived for the cloud emissivity, transmissivity and their product have the form

$$\left.\begin{aligned} \epsilon_\nu^c &= a_0 + a_1\Delta w + a_2\Delta w\Delta z \\ &\quad + a_3\Delta w(\Delta z)^2 + a_4\Delta z + a_5(\Delta z)^2 \\ T_\nu^c &= b_0 + b_1\Delta w + b_2\Delta w\Delta z \\ &\quad + b_3\Delta w(\Delta z)^2 + b_4\Delta z + b_5(\Delta z)^2 \\ \epsilon_\nu^c T_\nu^c &= c_0 + c_1\Delta w + c_2\Delta w\Delta z \\ &\quad + c_3\Delta w(\Delta z)^2 + c_4\Delta z + c_5(\Delta z)^2 \end{aligned}\right\}, \quad (10)$$

where coefficients a_i, b_i and c_i, which depend on frequency, are determined through the multiple regression program. The liquid water content and thickness have units of g cm^{-3} and km, respectively. The multiple correlation coefficients using Eq. (10) are better than 0.994 with standard deviations no larger than 0.01, indicating satisfactory fittings of cloud emissivity curves based on low-order polynomials. Coefficients a_i, b_i and c_i for SCAMS channels 1 and 2 using midlatitude summer climatological temperature and humidity profiles are listed in Table 1. The magnitude of these coefficients denote the relative importance of each term on the cloud emissivity and transmissivity values with respect to the cloud thickness and liquid water content variables as depicted in Eq. (10).

On substituting Eq. (10) into Eq. (9), calculations may be carried out for the brightness temperature. Comparisons with values obtained from our rigorous microwave radiative transfer program for the five SCAMS frequencies using climatological tropical and midlatitude summer and winter profiles reveal that the accuracy of the brightness temperature computed from the parameterized equation is within about 1%

TABLE 1. Coefficients, a_i, b_i and c_i for SCAMS channels 1 and 2.

ν	a_0	a_1	a_2	a_3	a_4	a_5	Correlation coefficient	Standard deviation
1	0.458×10^{-3}	0.360×10^{1}	-0.288×10^{0}	0	-0.184×10^{-1}	0.446×10^{-2}	0.999	0.003
2	-0.211×10^{-2}	0.648×10^{1}	-0.103×10^{1}	0.413×10^{-1}	-0.127×10^{-1}	0.955×10^{-2}	0.994	0.007

ν	b_0	b_1	b_2	b_3	b_4	b_5	Correlation coefficient	Standard deviation
1	0.101×10^{1}	-0.381×10^{1}	0.373×10^{0}	-0.202×10^{-1}	0	0	0.999	0.003
2	0.100×10^{1}	-0.744×10^{1}	-0.129×10^{1}	-0.663×10^{-1}	0.137×10^{-1}	-0.102×10^{-1}	0.994	0.010

ν	c_0	c_1	c_2	c_3	c_4	c_5	Correlation coefficient	Standard deviation
1	0.437×10^{-3}	0.348×10^{1}	-0.103×10^{1}	0.802×10^{-1}	-0.163×10^{-1}	0.160×10^{-1}	0.970	0.057
2	0.400×10^{-2}	0.506×10^{1}	-0.233×10^{1}	0.247×10^{0}	-0.138×10^{-2}	0.300×10^{-1}	0.915	0.118

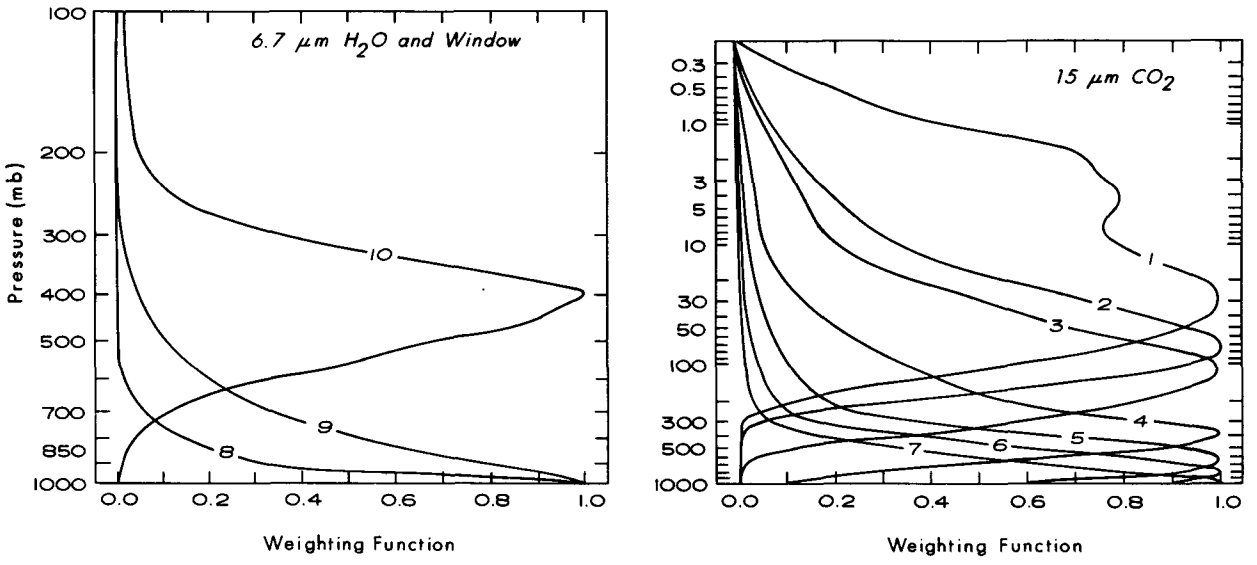

FIG. 3. Weighting functions of the HIRS 15 μm CO_2 and 6.7 μm H_2O channels.

over both land and ocean surfaces. Moreover, the last term in Eq. (9) for the water vapor and window channels contributes less than 0.1% (~0.3 K) of the total brightness temperature. Thus, it may be neglected in the numerical analysis.

3. Determination of high and low cloud top height, thickness and liquid water content from HIRS and SCAMS channels

a. Characteristics of HIRS and SCAMS channels

The Nimbus 6 HIRS instrument is a third-generation infrared radiation sounder. With a cross-course scan the HIRS provides nearly complete sounding coverage of the earth's atmosphere every 12 h. The instrument scans along a direction perpendicular to the subpoint track with the field of view of about 1.24°. There are 21 scan elements on each side of the subpoint track with a resolution of 23.8 km near nadir and 44.8 km at the extremes of the scan. The HIRS instrument scans IR radiation in 17 channels, which include seven channels in the 15 μm CO_2 band, five channels in the 4.3 μm CO_2 band, two water vapor channels at 6.8 and 8.6 μm, and three window channels at 11, 3.68 and 0.69 μm, respectively. The weighting functions for the temperature and water vapor sounding channels (for standard atmospheric conditions) are illustrated in Fig. 3. The peaks in this figure indicate the approximate location in the atmosphere from which its energy is derived.

The Scanning Microwave Spectrometer (SCAMS) is an advancement of the successful Microwave Spectrometer Experiment (NEMS) on Nimbus 5. SCAMS scans to either side of the subtrack and produces maps of atmospheric parameters with nearly full earth coverage every 12 h. The ground resolution of SCAMS is ~145 km at nadir and 330 km at 43° from nadir. The SCAMS consists of five microwave channels, each centered on a different frequency. The frequency of channel 1 lies on a water vapor line near 22 GHz. Channel 2 is an atmospheric window near 32 GHz, and channels 3, 4 and 5 are within the oxygen band near 54 GHz.

b. High cloud top height

In the following analysis, concerning the inference of the high cloud top height utilizing the 15 μm CO_2 band, we replace ν by i to indicate the channel number. Next we let the difference between the upwelling radiances for atmospheres containing no cloud [Eq. (8)] and a single-layer high cloud layer [Eq. (7)] be

$$\Delta A_i = I_i^{nc}(\infty) - I_i^{hc}(\infty) = (1 - T_i^{hc})\left[B_i(T_s)T_i(0) - B_i(T_h)T_i(z_h) + \int_0^{z_h} B_i(z)K_i(z)dz\right]. \quad (11)$$

To a good approximation, the high cloud transmissivity may be considered to be independent of the channel number in the 15 μm interval (Liou *et al.*, 1978), i.e., $T_i^{hc} \approx T_j^{hc}$, where i and j are two adjacent channels in the 15 μm CO_2 band. We define the ratio of the radiance differences for i and j channels as

$$H(z_h) = \frac{\Delta A_i}{\Delta A_j} = \frac{B_i(T_s)T_i(0) - B_i(z_h)T_k(z_h) + \int_0^{z_h} B_i(z)K_i(z)dz}{B_j(T_s)T_j(0) - B_j(T_h)T_k(z_h) + \int_0^{z_h} B_j(z)K_j(z)dz}. \quad (12)$$

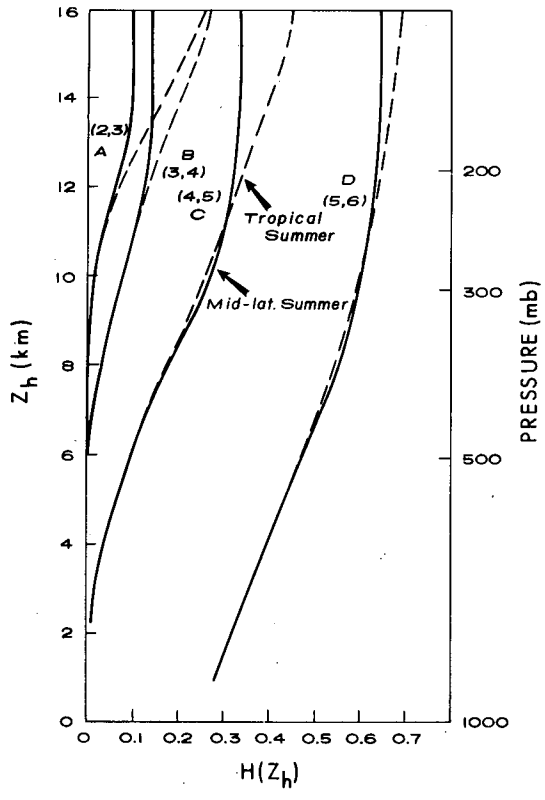

FIG. 4. Behavior of the H function (see text for the definition) as a function of the high cloud top height for four channel pairs in the 15 μm CO_2 band using two atmospheric profiles.

Because of the ratio, the H function is independent of the cloud opacity, and depends only on the weighting function of the channel, the cloud height, and the radiance profile from the surface to the cloud top. The selection of adjacent channels for cloud height inference has been discussed by McCleese and Wilson (1976).

The H function has been evaluated based on Eq. (12) utilizing the channel pair (2, 3), (3, 4), (4, 5) and (5, 6) of the Nimbus 6 HIRS 15 μm band for two climatological temperature profiles. The central wavenumbers for these channels are 679(2), 690(3), 702(4), 716(5) and 733 cm^{-1} (6). In Fig. 4, solid and dashed lines are for midlatitude summer and tropical summer profiles, respectively. It is seen that the H function is not a strong function of the atmospheric temperature profile up to the level of the tropopause. Moreover, from Eq. (12), we see that the H value depends only on z_h for a given radiance profile $B_r(z)$. Thus, the approximate relation between the H value and z_h may be constructed. From the definition of the H function [Eq. (12)], we require in the analysis the clear column radiance values which may be evaluated from radiosonde observations or an assumed climatological profile. The regions in which the cloud height z_h is a monotonous function of the H value are quite limited for curves A and B. Since channel 6 senses the lower part of the atmosphere, the low cloud has a significant effect on the determination of the H value for the channel pair (5, 6). It follows that this channel pair is not ideal for estimating the high cloud top height. The H value ranges from 0.02 to 0.32 when z_h is between 2.4 and 12 km for the C curve where z_h is less affected by the change of the H value, implying that the estimated z_h value would be more tolerable to observed errors in the H value. Thus, the channel pair (4, 5) is the best source for inferring the high cloud top height. From the C curve the cloud height z_h is approximately a linear function of H between 3 and 12 km which represents the approximate location of the cirrus cloud top. Thus, z_h may be determined by

$$z_h = d_0 + d_1 H, \tag{13}$$

where coefficients d_0 and d_1 derived through a regression analysis are 3.18 and 25.99, respectively, for the midlatitude summer climatological profile and 0.54 and 30.99, respectively, for the winter profile. The H value in Eq. (13) is to be evaluated from the form in Eq. (11) where $I^{hc}(\infty)$ is the satellite observed radiance for the channel with little contamination from low clouds and $I_i^{nc}(\infty)$ is the clear column radiance estimated from the assumed climatological temperature profile.

c. *High cloud thickness*

The HIRS water vapor channel in the 6.7 μm H_2O band is intended for the estimate of the water vapor concentration in the upper troposphere and for the detection of thin cirrus. The weighting functions for the HIRS temperature and water vapor channels are depicted in Fig. 3. An examination of the weighting function of the 6.7 μm water vapor channel (channel 10) reveals that this channel peaks at about 400 mb and has insignificant interference from the atmosphere below about 700 mb. After the cloud top height is estimated from the previous analysis, the cloud thickness may also be evaluated from the scheme described below.

For a thin cirrus cloud, the cloud transmissivity may be approximately expressed as an exponential function of the cloud optical thickness which is the product of the extinction coefficient and the geometric thickness. That is,

$$T_i^{hc} = \exp(-\beta_e \Delta z_h). \tag{14}$$

To determine the extinction coefficient $\beta_e(km^{-1})$, it is assumed that cirrus are composed entirely of ice. The single-scattering computation was made for the central wavenumber 1508.29 cm^{-1} in the water vapor band utilizing a theoretical ice cloud model developed by Liou (1972). A value of 1.326 km^{-1} is used for the extinction coefficient in this study.

Upon substituting Eq. (14) into Eq. (7), the effective cirrus cloud thickness is given by

$$\Delta z_h = -\frac{1}{\beta_e} \ln \times \left\{ \frac{I_i^{hc}(\infty) - \left[B_i(z_h)T_i(z_h) + \int_{z_h}^{\infty} B_i(z)K_i(z)dz \right]}{\int_0^{z_h} B_i(z)K_i(z)dz - B_i(z_h)T_i(z_h)} \right\}. \quad (15)$$

It should be noted that the analysis presented here assumes an overcast cloudy condition. Thus, the cloud thickness derived here may be thought of as an effective thickness in the event that the cloud covers partly in the field-of-view of the radiometer. Because of the strong water vapor absorption in this channel, low clouds below 700 mb have little effect on the observed radiation at the satellite point. Thus, the upwelling radiance at the 6.7 μm H_2O channel is only affected by the high cloud so that the term I_i^{hc} in Eq. (7) may be regarded as the satellite observed radiance. Since the cloud top height z_h has been estimated from the foregoing analysis, the cirrus cloud thickness Δz_h may be subsequently determined using Eq. (15).

d. Low cloud top height

To determine the low cloud top height, we rewrite the infrared radiative transfer denoted in Eq. (5) in the form

$$I_i^c(\infty) = T_i^{hc}T_i^{lc}I_i^3 + T_i^{hc}I_i^2 + I_i^1, \quad (16)$$

where I_i^3, I_i^2 and I_i^1 are respective bracketed terms appearing in Eq. (5). For the HIRS channels, the contribution to the upwelling radiance from the first term on the right-hand side of Eq. (16) is insignificant, due to the large extinction of IR radiation in water clouds. For example, if a thick low cloud deck has a thickness of 3 km, the cloud transmissivities T_i^{lc} for channels 8 and 10 are 4.6×10^{-16} and 7.2×10^{-20}, respectively. If, on the other hand, a thin low cloud with a thickness of 0.5 km is considered, the cloud transmissivities for these two channels will increase to 2.8×10^{-3} and 6.4×10^{-4}, respectively. However, because the term I_i^3 also is a small value, the first term contribution in Eq. (16) will still be less than 0.1%. Thus, Eq. (16) may be written in the form

$$I_i^c(\infty) - I_i^1 \approx T_i^{hc}I_i^2. \quad (17)$$

To infer the low cloud top height we select the 6.7 μm water vapor channel (channel 10) which senses the atmosphere above about 700 mb and the window channel (channel 8) which has the weighting function peak at the surface. Since the transmissivities of ice clouds at 6.7 and 11 μm are about the same, we may define the function such that

$$F(z_h, z_l) = \frac{I_{10}^2}{I_8^2} = \frac{I_{10}^c(\infty) - I_{10}^1}{I_8^c(\infty) - I_8^1}. \quad (18)$$

The purpose of performing the ratio for the two channel radiances is to eliminate the cloud transmissivities for these two channels, on the one hand, and to minimize the atmospheric water vapor and temperature effects on the other. As is evident from Eq. (16), the F function depends on the high cloud top height, low cloud top height, and weighting functions and radiance profiles of the water vapor and window channels. Among these variables, the high cloud top height will be determined from the previous analysis. Furthermore, weighting functions and radiance profiles may be approximately estimated from the available radiosonde observations or from climatological temperature and humidity data. From $F = I_{10}^2/I_8^2$, there will be a unique relationship through a low-order polynomial in a form $\sum_{i=0}^{2} c_i F^i$ between the function F and the low cloud top height z_l, where c_i are coefficients determined in the numerical program. Subsequently, z_l can then be determined by knowing the value of F which is to be estimated from $F = (I_{10}^c - I_{10}^1)/(I_8^c - I_8^1)$.

e. Surface emissivity and liquid water content

The low cloud information is contained in Eq. (9) through values of ϵ_i^c and T_i^c, which in turn are functions of the liquid water content and cloud thickness as shown in Eq. (10). Substituting Eq. (10) into Eq. (9) and neglecting the last term as described previously, we obtain after a number of mathematical manipulations

$$T'_B(i) = [u_1 + u_2 z_l + u_3 z_l^2]\Delta w + u_0 + u_4 z_l + u_5 z_l^2, \quad (19)$$

where

$$T'_B(i) = \left[\tilde{T}_B(i) - \int_{z_l}^{\infty} T(z)K_i(z)dz \right][T_i(z_l)]^{-1}, \quad (20)$$

$$u_j = a_j T_c + b_j T_s \epsilon_i + c_j T_c(1 - \epsilon_i), \quad j = 0, 1, 2, 3, 4, 5, \quad (21)$$

where a_j, b_j and c_j are defined in Eq. (10), and listed in Table 1. It should be noted that while the last term in Eq. (9), which contributes less than 0.1% of the total brightness temperature, has been omitted in the parameterization, the surface reflection contribution is still included through the second term in Eq. (9). If the temperature and humidity profiles are prescribed and the cloud thickness or cloud top height z_l is determined from previous analysis, then $T'_B(i)$ may be estimated from the observed brightness temperature $\tilde{T}_B(i)$. Furthermore, if the surface emissivity

TABLE 2. Coefficients a and b for cloud thicknesses between 0 and 5 km.

Δz (km)	a	b	Correlation coefficient	Standard deviation
$0 \le \Delta z < 1$	−0.9583	0.1957×10^1	1.000	0.001
$1 \le \Delta z < 2$	−0.8299	0.1818×10^1	0.999	0.003
$2 \le \Delta z < 3$	−0.7334	0.1708×10^1	0.999	0.003
$3 \le \Delta z < 4$	−0.6480	0.1605×10^1	0.998	0.005
$4 \le \Delta z < 5$	−0.5721	0.1510×10^1	0.997	0.007

ϵ_i is estimated from the SCAMS data for the water vapor and window channels utilizing a method to be discussed in this section, the liquid water content can then be obtained from Eq. (19) in the form

$$\Delta w = \{T'_B(i) - [u_0 + u_4 z_l + u_5 z_l^2]\}/ [u_1 + u_2 z_l + u_3 z_l^2]. \quad (22)$$

We shall now describe the procedure for determining the surface emissivity from SCAMS channels 1 and 2. For these two frequencies, the terms corresponding to the ground reflection from the clear column emission above the cloud top may be neglected. Consequently, we may rewrite the parameterized microwave radiation transfer equation denoted in Eq. (9) to obtain an expression for the surface reflectivity in the form

$$R_i = \frac{(T_s - T_c)T_i^c T_i^0 + T_i^0(T_c - T_{ei}) + T_{ei} - \tilde{T}_B(i)}{T_s T_i^c T_i^0}, \quad i = 1, 2, \quad (23)$$

where R_i is the surface reflectivity, T_i^0 the clear-column transmissivity from the top of the atmosphere to the upper boundary of the low cloud layer, and T_{ei} an equivalent atmospheric emission temperature which is approximately given by $T_{ei} \approx 0.94 \times T(850$ mb) for the SCAMS water vapor and window channels. Note that the surface emissivity $\epsilon_i = 1 - R_i$. Using the approximation for T_{ei} the accuracy of computing $\tilde{T}_B(i)$ in Eq. (23) is within 0.5%. Also note that we have replaced ϵ_i^c by $(1 - T_i^c)$. According to Waters *et al.* (1975) $R_2/R_1 = r = 1$, for land and $r = 0.97$ for a calm water surface. In addition, on examining the computational results from the microwave radiation transfer program, we find that to a good approximation the cloud transmissivities for the water vapor and window channels are related through a linear equation within a cloud thickness increment of 1 km and can be expressed by $T_2^c = a + bT_1^c$, where a and b are coefficients determined from regression analyses and are listed in Table 2. Thus, the surface reflectivities and the cloud transmissivities can be obtained from $\tilde{T}_B(1)$ and $\tilde{T}_B(2)$ through Eq. (23). The approximation in deriving this equation, i.e., omitting the contribution of the ground reflection of the gaseous emission above the cloud denoted in the last term of Eq. (9), is consistent with that used in derived Eq. (23). Again, the ground reflection contribution is included through the cloud downward emission depicted in the second term of Eq. (9).

4. Results from theoretical analyses

In this section, a hypothetical cloudy atmosphere is constructed and numerical calculations of atmospheric parameters are performed in order to test the validity of the foregoing deviations. Numerical procedures involving sequential computations for cloud parameters and the error analysis for theoretical calculations will be presented.

a. Numerical procedures

If the observed radiances for a discrete set of infrared and microwave sounding frequencies are known, we can proceed to determine cloud parameters using the numerical procedures outlined below:

1) Obtain temperature and humidity profiles from radiosonde observations or from climatological data.
2) Compute the transmittance and weighting function profiles for HIRS and SCAMS channels from the known temperature and humidity profiles.
3) Insert the satellite observed value and clear column radiance into Eq. (11) and evaluate the H function from the equation $H = \Delta A_i/\Delta A_j$ using channels 4 and 5 of the HIRS 15 μm CO_2 band. The high cloud top height z_h can then be calculated by means of Eq. (13).
4) Insert the values of $T(z)$ and z_h into Eq. (15) and compute the high cloud thickness using the HIRS strong water vapor band.
5) Substitute $T(z)$ and z_h into Eq. (16) and calculate the F function denoted in Eq. (18) employing the HIRS window and water vapor channels. Subsequently, the low cloud top height z_l which is a function of F may be obtained.
6) Once z_l is known, we may compute the surface reflectivity R_1 for channel 1 based on Eq. (23).
7) By substituting $T(z)$, z_l and ϵ_i into Eq. (22), the liquid water content Δw can be readily obtained.

b. Error analysis

In this section, the error sensitivity of the aforementioned numerical procedures will be examined. Different percentages of the measurement error are introduced into theoretical calculations, and results of the errors generated in the sequential computations are analyzed.

In the error analysis, a hypothetical atmosphere containing a two-layered cloud is constructed using a midlatitude summer climatological profile. The cirrus cloud top is assumed to be located at 300 mb

TABLE 3. Error sensitivity analyses for the sequential computation of the cirrus top height z_h, thickness Δz_h, low cloud top height z_l, surface emissivity of the SCAMS channel 1, and liquid water content over land and ocean surfaces by imposing different percentages of maximum random errors. S.D. indicates standard deviation.

		Maximum random error (%)					
		0.0	0.5	1.0	1.5	2.0	2.5
z_h (km)	mean	9.28	9.31	9.46	9.48	9.38	9.53
	S.D.	0.51×10^{-1}	0.80×10^{-1}	0.11	0.19	0.21	0.35
Δz_h (km)	mean	1.08	1.08	1.06	1.07	1.09	1.10
	S.D.	0.90×10^{-2}	0.15×10^{-1}	0.17×10^{-1}	0.19×10^{-1}	0.20×10^{-1}	0.24×10^{-1}
z_l (km)	mean	2.03	2.22	1.97	2.30	2.35	2.08
	S.D.	0.30×10^{-2}	0.14	0.18	0.29	0.31	0.32
ϵ_1 (land)	mean	0.97	0.96	0.95	0.90	0.89	0.89
	S.D.	0.43×10^{-2}	0.52×10^{-2}	0.92×10^{-2}	0.20×10^{-1}	0.33×10^{-1}	0.49×10^{-1}
LWC_1 (g cm^{-2})	mean	0.69×10^{-1}	0.74×10^{-1}	0.76×10^{-1}	0.91×10^{-1}	0.12×10^{0}	0.11×10^{0}
	S.D.	0.35×10^{-2}	0.91×10^{-2}	0.11×10^{-1}	0.29×10^{-1}	0.53×10^{-1}	0.35×10^{-1}
LWC_2 (g cm^{-2})	mean	0.76×10^{-1}	0.81×10^{-1}	0.10×10^{0}	0.97×10^{-1}	0.98×10^{-1}	0.90×10^{-1}
	S.D.	0.48×10^{-2}	0.90×10^{-2}	0.17×10^{-1}	0.15×10^{-1}	0.21×10^{-1}	0.35×10^{-1}
ϵ_1 (ocean)	mean	0.48	0.44	0.43	0.43	0.47	0.45
	S.D.	0.36×10^{-2}	0.93×10^{-2}	0.11×10^{-1}	0.20×10^{-1}	0.27×10^{-1}	0.33×10^{-1}
LWC_1 (g cm^{-2})	mean	0.65×10^{-1}	0.66×10^{-1}	0.59×10^{-1}	0.56×10^{-1}	0.53×10^{-1}	0.45×10^{-2}
	S.D.	0.25×10^{-3}	0.42×10^{-2}	0.39×10^{-2}	0.48×10^{-2}	0.72×10^{-2}	0.99×10^{-2}
LWC_2 (g cm^{-2})	mean	0.71×10^{-1}	0.73×10^{-1}	0.70×10^{-1}	0.64×10^{-1}	0.52×10^{-1}	0.52×10^{-1}
	S.D.	0.47×10^{-3}	0.80×10^{-3}	0.18×10^{-2}	0.85×10^{-2}	0.97×10^{-2}	0.10×10^{-1}

(~9.36 km) with a thickness of 1 km, while the low cloud top height is placed at 780 mb (~2.23 km) and a total liquid water content of 0.07 g cm^{-2} is used. The "observed" IR upwelling radiances for the HIRS channels are computed from Eq. (5), while the "observed" microwave upwelling brightness temperatures for the SCAMS channels are calculated from Eq. (9). In calculating the observed infrared radiances and microwave brightness temperatures, we introduce a Gaussian random noise distribution to the temperature and water vapor profiles. These random noises, which are to be added to 40 values of temperature and water vapor concentration, are determined by an inverse Gaussian probability distribution function. The standard deviations used for the temperature and water vapor profiles are 2 K and 20%, respectively. After this is done, we then impose some artificial measurement errors onto the observed values. The measurement error (which is not larger than a prescribed number) is randomly selected by a random number generator for each channel. Upon imposing different percentages of maximum random errors in each observed value, computations of the cloud parameters and surface emissivities are subsequently carried out. In order to obtain physically meaningful solutions, the program is set up in such a manner that cases were eliminated if the computed surface emissivity was outside the range between 0.4 and 1.0, or if the computed liquid water content was a negative value. In the error analysis exercises, the dropout rate for the 0, 0.5, 1, 1.5, 2 and 2.5% maximum random errors were 0, 7, 12, 16, 21 and 24%, respectively. For each percentage of maximum random error, there are at least 25 cases presented so that the results are statistically representative.

Results of the sequential calculations for the cirrus cloud top height, cloud thickness, low cloud top height, surface emissivities and cloud liquid water content over both land and ocean surfaces are given in Table 3 and illustrated in Fig. 5.

In Table 3, the mean values and standard deviations for a sample of at least 25 cases for each maximum random error are listed for maximum random errors ranging from 0 to 2.5%. The mean computed cirrus top height z_h has values ranging from 9.28 to 9.53 km, which are close to the assumed value as shown in this table as well as in Fig. 5a. Note that even without imposing random errors on the observed values, the computed high cloud top height of 9.28 km is slightly lower than the assumed value of 9.36 km. This is caused by the small interference of the low cloud on the HIRS channels 4 and 5. In Fig. 5a, the dashed line represents the computed cirrus thickness Δz_h, which is generally overestimated. The computed low cloud top height z_l is denoted by the solid line in Fig. 5b. As a result of overestimating Δz_h (without imposing any random error) in the foregoing calculation, the computed z_l with a value of 2.024 km is slightly lower than the assumed value of 2.228 km. This is due to the compensating effects in

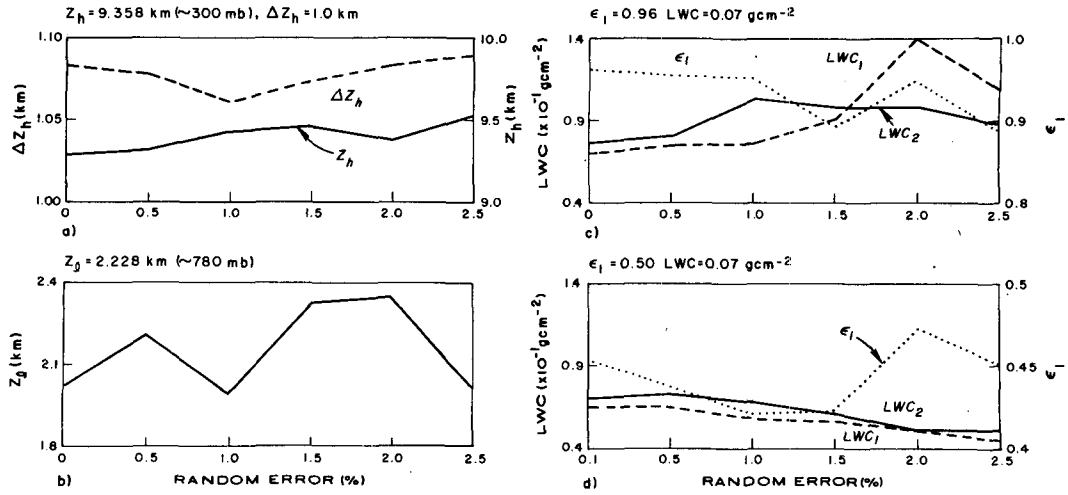

FIG. 5. Hypothetical error analyses for the retrieval of the cirrus cloud top height and thickness (a), low cloud top height (b), microwave emissivity and liquid water content over land (c) and over water (d).

which Δz_h is overestimated, leading to an underestimation for the low cloud thickness (or height) in order to produce the same upwelling radiance. For the random errors used in this study, maximum deviations of the mean calculated Δz_h and z_l from real values are within 0.087 and 0.394 km, respectively, as depicted in Table 3.

Regarding the calculation of surface emissivities over land using SCAMS channels, we display the result for channel 1 in Fig. 5c (dots). It is apparent that ϵ_1 is nonlinear with respect to the percentage of measurement errors and that ϵ_1 is not linear to variations in the low cloud thickness. In Table 3, we see that, without random error, the mean computed value for ϵ_1 is 0.971, which is larger than the assumed value of 0.960. Again, this may be due to the compensating effect which counterbalances the underestimation of the low cloud thickness such that the same upwelling brightness temperatures may be produced. Note that in the microwave region, the satellite radiometer sees through most of the high clouds and detects low clouds and ground characteristics. Overestimation of ϵ_1 directly affects the calculation of liquid water content (LWC). To examine the influence of ϵ_1 on LWC, we compute LWC based on two different sets of surface emissivity; one is the assumed value used in this theoretical model (0.96 for channels 1 and 2) and the other is the preceeding computed value. Results of the calculations are also exhibited in Fig. 5c.

In Fig. 5c, LWC_1 (dashed line) represents the mean LWC computed by using assumed emissivity values, and LWC_2 (solid line) is estimated from the present retrieval scheme. Since 0.07 g cm^{-2} is the prescribed solution for LWC, LWC_1 is evidently a better result than LWC_2 for a maximum random error below 1.5% as shown in Fig. 5c. However, it appears that the result of LWC_2 is more stable than LWC_1 as the percentage of random error continues to increase. The stable condition in the case of LWC_2 is apparently due to the consequence of decreasing surface emissivity, which in effect reduces the rate of increasing LWC. The compensating effects in the calculations for cloud and emissivity parameters are the fundamental reason for the success of the sequential numerical computations. Results of mean LWC_2 range from 0.076 to 0.10 g cm^{-2} as listed in Table 3. This range appears to be reasonable in view of the difficulty encountered in deriving the liquid water content over land from any remote sensing or *in-situ* technique.

The last three columns in Table 3 and Fig. 5d show the error sensitivity analysis for the microwave surface emissivity and liquid water content over a water surface which is assumed to have an emissivity of 0.5. Resulting emissivities corresponding to various random errors derived from the present retrieval program are shown to be underestimated by about 0.07–0.03. These consistent discrepancies may well be caused by the neglect of the term corresponding to the ground reflection from the cloud in the parameterization of surface emissivity calculations. In a manner similar to the case over land, two calculations for LWC were carried out. LWC_1 (dashed line) shown in Fig. 5d represents the mean liquid water content derived from an assumed emissivity value of 0.5 for SCAMS channel 1, while LWC_2 (solid line) is directly computed from the present retrieval scheme. We see that LWC_1 is underestimated, whereas LWC_2 is slightly overestimated as compared to the assumed LWC of 0.07 g cm^{-2} even without imposing a measurement error. As the measurement error increases, values of LWC_2 and LWC_1 decrease. The LWC_2 curve shows better results due to the adjustment of the computed surface emissivity. We also note that for a given maximum random error, the standard deviations for the computed LWC are consistently smaller for the ocean surface case than for the land surface case.

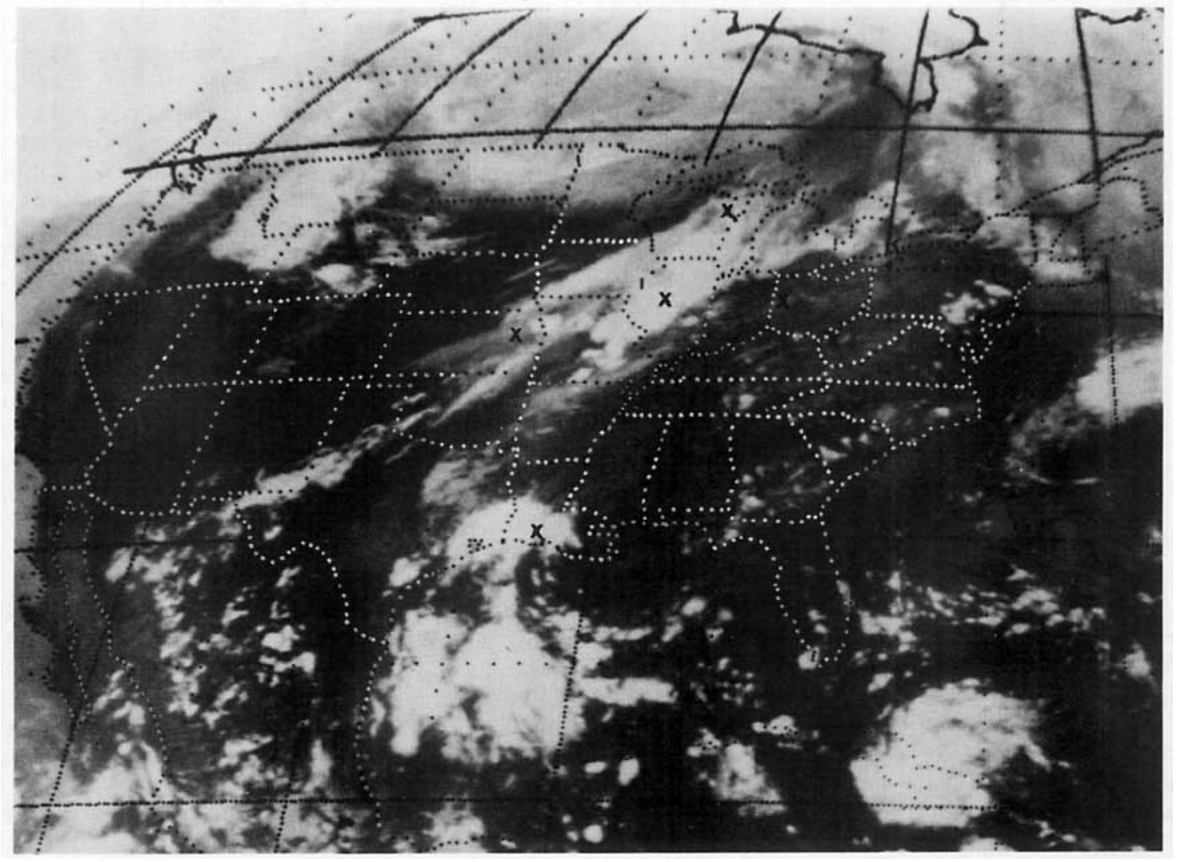

FIG. 6. GOES infrared imagery for 1900 GMT 25 August 1975. The crosses indicate the stations chosen.

5. Applications to Nimbus 6 data

On the basis of the previous analysis and illustrations it is evident that a proper combination of IR and microwave measurements may be successfully used to recover the cloud parameters. It appears desirable and important to apply the developed retrieval scheme to real satellite data to investigate its applicability. In order to have some confidence in the computed cloud parameters, we have collected and documented the observed atmospheric parameters in conjunction with the colocated satellite data. These atmospheric parameters were derived from the surface and upper air observations, radar echoes, precipitation, satellite pictures and other relevant synoptic features. A case, which was associated with summertime convection over the United States during 25 August 1975, was selected in this study.

For the 25 August 1975 case, we focus on the areas over the north-central United States where significant activities took place. The GOES IR satellite picture that was available at the time of the Nimbus 6 orbital pass on 25 August is shown in Fig. 6. The prominent cloud feature was the cyclone over Canada with a well-defined spiral pattern around the surface low center. A frontal cloud band extended from approximately Lake Michigan to Kansas with numerous convective clouds ahead of the front over Missouri. Another area of cloudiness was located over Louisiana and eastern Texas and was associated with moist southerly flow from the Gulf of Mexico. Cumulus cloud lines with anticyclonic curvature were present in the high pressure center over the southeastern United States.

The horizontal mapping of the calculated liquid water content using the available HIRS and SCAMS data is shown in Fig. 7. Results of liquid water content values depicted in this figure generally coincide with the cloud bands shown in the GOES IR image (Fig. 6) and radar echoes at 1835 GMT. The liquid water for the southern cloud mass, which is greater than that for the frontal band, is associated with moist air from the Gulf of Mexico. Several individual cases in which conventional data are available for comparison are briefly described below.

Surface reports indicated the rainfall rate at Lake Charles, Louisiana was about 1 mm h^{-1} at 1800 (all times GMT). The computed liquid water content and low cloud thickness using satellite data at 1716 are 0.219 g cm^{-2} and 4.39 km, respectively. The computed liquid water content, when converted to the rainfall rate utilizing the Marshall-Palmer size distribution, is equivalent to 7 mm h^{-1}, which is much larger than the rainfall rate observed at the surface.

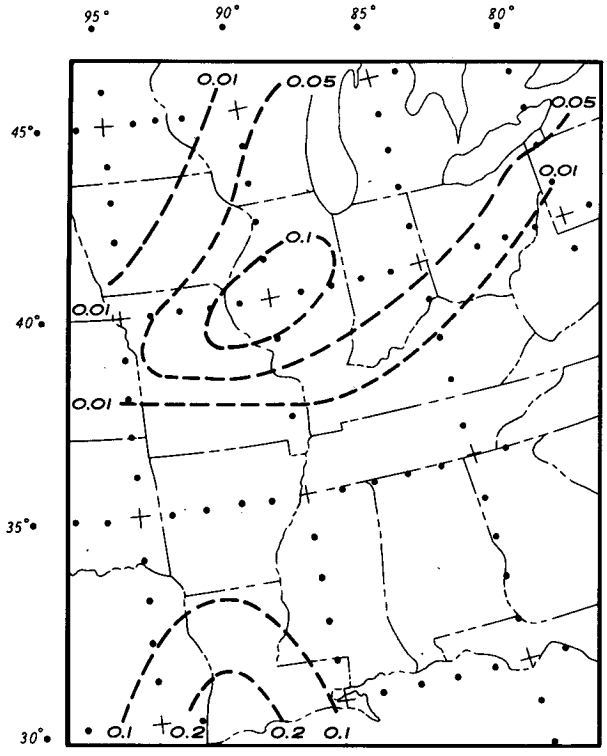

FIG. 7. Mapping of atmosphere liquid water content (g cm^{-2}) for the summertime convection case (25 August 1975) using the Nimbus HIRS and SCAMS data.

Since surface, radar and synoptic reports indicate strong convective activity in the area, the observed cumulonimbus clouds could have contained large cloud droplets. The computed surface emissivity with a value of 0.93 indicates that Lake Charles area might have a wet surface at the time of satellite passage.

At 1719 GMT 25 August, according to an 1800 surface report and 1900 GOES IR imagery, Topeka, Kansas was covered by a low cloud deck with thin cirrus aloft. Inspection of the sequential surface maps reveals a major cold front passed Topeka at about 1200. As described previously, clouds in the post frontal region tend to be less convective and contain smaller amounts of moisture. Thus, the computed cloud liquid water content of 0.032 g cm^{-2} with 4.64 and 0.13 and 10.89 km for low and high cloud thicknesses, and high cloud top height, respectively, appears to agree well with synoptic observations.

The precipitation report from Peoria, Illinois at 1800 indicated a rainfall rate of 0.5 mm h^{-1}. The calculated liquid water content was 0.118 g cm^{-2}, which is equivalent to about 4.6 mm h^{-1} rainfall rate. Again, the larger computed value for the cloud liquid water content may be associated with a well-developed convective cloud.

The strong frontal activity at Green Bay, Wisconsin or Dayton, Ohio produced no precipitation. The computed cloud liquid water content for the Green Bay case is 0.061 g cm^{-2} and the computed surface emissivity 0.922, which is lower than the normally estimated value over dry land (0.96). This is because the satellite field-of-view was partially covered by the water surface. The calculated values show that the cloud liquid water content at Huntington is about 0.006 g cm^{-2}. The small cloud liquid water content obtained for this case might be due to the lack of moisture supply, since the station was far east of the very active frontal zone.

In summary, we have applied the cloud sounding technique developed from the parameterization of infrared and microwave radiative transfer to Nimbus 6 HIRS and SCAMS data. The satellite retrieval cloud parameters from selected infrared and microwave channels appear to be in qualitative agreement with the available synoptic, radiosonde, surface and radar reports.

6. Conclusion

In this study, a numerical method for computing cloud parameters utilizing a combination of infrared and microwave channels from the Nimbus 6 satellite has been developed. We first formulate parameterized equations to simulate IR upwelling radiances in multiple-layered cloudy atmospheres. The high cloud top height and thickness, and low cloud top height are subsequently derived from a selected set of HIRS longwave CO_2, window and water vapor channels. We then further develop parameterized equations to simulate microwave upwelling brightness temperature in cloudy atmospheres. Moreover, by means of parameterized equations, surface emissivities of the SCAMS channels and the atmospheric liquid water content are evaluated.

In order to examine the validity of the theoretical parameterization programs for the retrieval of atmospheric parameters, a number of hypothetical experiments have been performed to test the sensitivity to errors in the calculations. By imposing various degrees of random errors on the assumed temperature and water vapor profiles, the theoretically "observed" data are generated. Measurement errors are then introduced onto the "observed" data and numerical experiments for recovering cloud parameters are subsequently carried out. Resulting cloud parameters retrieved from the present program are found to be reasonably accurate by comparison with theoretically assumed solutions.

Furthermore, we have applied the present retrieval technique to realistic atmospheres by utilizing Nimbus 6 HIRS and SCAMS data in which various cloudy conditions were chosen. These cloudy conditions include high and low cloud overcasts, and low cloud obstructions. Precipitation was in the form of either rain or snow. Results of retrieval experiments appear to agree qualitatively with those noted from the synoptic report, radar echoes, precipitation summary,

satellite IR imageries and radiosonde observations at the time of the satellite passage. Since detailed information concerning cloud parameters (such as cloud thickness, liquid water content, etc.) were not available, the reliability of the retrieval programs needs to be further verified. Unfortunately, verification of the satellite cloud sensing techniques requires carefully designed field experiments in which reliable cloud properties, such as phase, size distribution, liquid water/ice content and thickness, may be obtained from aircraft observations under the satellite pass.

Acknowledgments. This research was supported in part by the Air Force Geophysics Laboratory under Contract F19628-78-C-0130 and by the Atmospheric Research Section of the National Science Foundation under Grant ATM 81-09050. During the final stage of the research work, Mike Yeh was supported by the Research Visiting Members Program of CIRA at Colorado State University. We thank Dr. W. Smith and a number of reviewers in the JAS and JAM review process for offering numerous comments and suggestions which led to significant improvement on the paper, and Ms. Sharon Bennett for typing and editing various versions of the revised manuscript.

REFERENCES

Chahine, M. T., H. H. Aumann and F. W. Taylor, 1977: Remote sensing of cloudy atmospheres. Part III: Experimental verification. *J. Atmos. Sci.*, **34,** 758–765.

Feddes, R. G., and K. N. Liou, 1978: Atmospheric ice and water content derived from parameterization of Nimbus 6 High Resolution Infrared Sounder data. *J. Appl. Meteor.*, **17,** 536–551.

Grody, N. C., 1976: Remote sensing of atmospheric water content from satellites using microwave radiometry. *IEEE Trans. Antennas Propagat.*, **AP-24,** 155–162.

——, A. Gruber and W. C. Shen, 1980: Atmospheric water content over the tropical Pacific derived from the Nimbus 6 scanning microwave spectrometer. *J. Appl. Meteor.*, **19,** 986–996.

Houghton, J. T., and G. E. Hunt, 1971: The detection of ice clouds from remote measurements of their emission in the far infrared. *Quart. J. Roy. Meteor. Soc.*, **96,** 1–17.

Liou, K. N., 1972: Light scattering by ice clouds in the visible and infrared: A theoretical study. *J. Atmos. Sci.*, **29,** 524–536.

——, 1977: Remote sensing of the thickness and composition of cirrus clouds from satellites. *J. Appl. Meteor.*, **16,** 91–99.

——, and A. D. Duff, 1979: Atmospheric liquid water content derived from parameterization of Nimbus 6 scanning microwave spectrometer data. *J. Appl. Meteor.*, **18,** 99–103.

——, T. L. Stoffel, R. G. Feddes and J. T. Bunting, 1978: Radiative properties of cirrus clouds in NOAA 4 VTPR channels: Some explorations of cloud scenes from satellites. *Pure Appl. Geophys.*, **116,** 1007–1029.

Marshall, J. S., and W. M. Palmer, 1948: The distribution of raindrops with size. *J. Meteor.*, **5,** 165–166.

McCleese, D. J., and L. S. Wilson, 1976: Cloud top heights from temperature sounding instruments. *Quart. J. Roy. Meteor. Soc.*, **102,** 781–790.

Smith, W. L., and H. M. Woolf, 1976: The use of eigenvectors of statistical covariance matrices for interpreting satellite sounding radiometer observations. *J. Atmos. Sci.*, **33,** 1127–1140.

Staelin, D. H., K. F. Kunzi, R. L. Pettyjohn, R. K. L. Poon and R. W. Wilcox, 1976: Remote sensing of atmospheric water vapor and liquid water with the Nimbus 5 microwave spectrometer. *J. Appl. Meteor.*, **15,** 1204–1214.

Waters, J. W., K. F. Kunzi, R. L. Pettyjohn, R. K. L. Poon and D. H. Staelin, 1975: Remote sounding of atmospheric temperature profiles with the Nimbus 5 microwave spectrometer. *J. Atmos. Sci.*, **32,** 1953–1969.

Wielicki, B. A., and J. A. Coakley, Jr., 1981: Cloud retrieval using infrared sounder data: Error analysis. *J. Appl. Meteor.*, **20,** 157–169.